

Two-photon speckle illumination for super-resolution microscopy

AWOKE NEGASH,¹ SIMON LABOUESSE,¹ PATRICK C. CHAUMET,¹ KAMAL BELKEBIR,¹ HUGUES GIOVANNINI,¹ MARC ALLAIN,¹ JÉRÔME IDIER,² AND ANNE SENTENAC^{1,*}

¹Aix Marseille Université, CNRS, Centrale Marseille, Institut Fresnel, UMR 7249, 13013 Marseille, France

²LS2N, CNRS, UMR 6004, 44321 Nantes, France

*Corresponding author: anne.sentenac@fresnel.fr

Received 25 January 2018; revised 18 April 2018; accepted 18 April 2018; posted 19 April 2018 (Doc. ID 320626); published 25 May 2018

We present a numerical study of a microscopy setup in which the sample is illuminated with uncontrolled speckle patterns and the two-photon excitation fluorescence is collected on a camera. We show that, using a simple deconvolution algorithm for processing the speckle low-resolution images, this wide-field imaging technique exhibits resolution significantly better than that of two-photon excitation scanning microscopy or one-photon excitation bright-field microscopy. © 2018 Optical Society of America

OCIS codes: (180.6900) Three-dimensional microscopy; (110.6150) Speckle imaging; (180.2520) Fluorescence microscopy.

<https://doi.org/10.1364/JOSAA.35.001028>

1. INTRODUCTION

Two-photon excitation (2PE) microscopy is widely used for imaging deep into scattering tissues [1]. In a standard 2PE microscope, a sample is scanned with a focused pulsed beam and all of the emitted two-photon fluorescence is collected on a large detector. To avoid the slow scanning process, several wide-field two-photon schemes have also been developed [2–5]. These approaches have been made possible by an increase in the power of the exciting pulsed laser. In these configurations, 2PE fluorescence is excited on a wide surface in the focal plane of the objective and collected on a camera. Both the scanning and wide-field modes exhibit similar resolution of about 300 nm transversely and 1 μm axially [1].

Recently, it has been proposed to introduce structured illumination and numerical reconstructions in 2PE microscopy in order to ameliorate the resolution [6–8]. These approaches yield promising results but are plagued by the necessity, inherent to all structured illumination super-resolution techniques, to strictly control the illumination patterns. In this work, we propose to adapt to 2PE excitation the speckle imaging technique that has been developed in the framework of one-photon (1PE) excitation microscopy [9]. We show, on synthetic data, that this approach permits a significant improvement of resolution while releasing the constraints on the knowledge of the illuminations. The paper is organized as follows: in a first section, we discuss the resolution gain in speckle imaging and describe the reconstruction algorithm. In a second part, we focus specifically on 2PE speckle microscopy and analyze its transverse and axial resolutions.

2. PRINCIPLES OF SPECKLE IMAGING

Speckle imaging consists of recording several images of a sample under uncontrolled speckle illuminations and processing them to form a super-resolved map of the sample. In practical applications, the speckles can be obtained by moving a diffuser through the laser path in front of the microscope objective as shown in Ref. [9]. The key point of this approach lies in the ability of the reconstruction procedure to extract fine details of the sample from the low-resolution speckle images.

A. Super-resolution Capacity of Speckle Imaging

We consider a simple model of a speckle image M ,

$$M = \rho I * h, \quad (1)$$

where I is the illumination, ρ is the sample fluorescence density, h is the collection point-spread function, and $*$ stands for the convolution operator. When I is a known constant, M depends on the sample spectrum within the support of the optical transfer function (OTF), \hat{h} , where \hat{a} is the 3D Fourier transform of a . When I is inhomogeneous, M depends on the sample spectrum within the support of $\hat{h} \star \hat{I}$,

$$[\hat{h} \star \hat{I}](\mathbf{k}) = \int \hat{h}(\mathbf{k} + \mathbf{u}) \hat{I}(\mathbf{u}) d^3 u, \quad (2)$$

which is larger than the support of \hat{h} . In classical structured illumination microscopy (SIM), when the illuminations are known, the sample spectrum can be identified on the union of the supports of \hat{I} and \hat{h} . In speckle imaging, when only

the statistics of I are known, the identification of $\hat{\rho}$ over this enlarged support is an open question.

Recently, a mathematical study analyzed the information content of the mean and covariance of speckle images [10] (in the asymptotic limit of an infinite number of speckles). Assuming that the ensemble average of the speckles $\langle I \rangle$ is a constant, the spectrum of ρ on the support of \hat{h} can be easily inferred from the mean of the speckle images. More importantly, it was shown that if the support of \hat{I} is included in that of \hat{h} , the sample spectrum can be retrieved from the image covariance on the support of $\hat{I} \star \hat{I}$. When the speckles have the same Fourier support as the OTF, one retrieves the two-fold resolution gain of classical SIM. On the other hand, if the support of \hat{I} extends outside that of \hat{h} , the identification of the sample spectrum on a domain larger than that of \hat{h} is not guaranteed anymore. This analysis consolidates several observations made in one-photon speckle microscopy in which increasing the support of \hat{I} beyond that of the collection OTF had a negative impact on the final resolution [9,11]. However, while indicating some possible difficulties, this lack of guarantee does not prejudice the outcome of all reconstruction algorithms, in particular, of those using *a priori* information on the sample.

B. Reconstructing a Super-resolved Image in Speckle Microscopy: Blind-SIM Algorithms

In the last 5 years, different inversion schemes have been proposed to process low-resolution speckle images into a super-resolved estimation of a sample. In Ref. [9], both the sample and the illuminations are estimated using the minimization of the L_2 distance between the data and the model. The positivity of the unknowns and the assumption of a homogeneous speckle average reduce the number of unknowns and render the minimization tractable. In Ref. [10], a maximum likelihood estimation of the sample is obtained from the mean and covariance of the images, assuming the mean and covariance of the speckles are known. A localization technique, adapted to the imaging of binary objects, has been developed in Ref. [12]. However, the separate deconvolution approaches developed in Refs. [11,13] are presently the simplest and fastest techniques. They consist of de-convolving each speckle image under positivity or sparsity constraints and forming their mean to estimate the sample. In this procedure, the super-resolution stems from the activation of the positivity or sparsity constraints, which happens more frequently when fluorescence has been excited with a speckle than with homogeneous light [11,13]. Hereafter, all sample reconstructions are performed with the separate deconvolution scheme with the positivity constraint presented in Ref. [13] and briefly sketched in the Appendix A. Note that similar results have been obtained with the deconvolution scheme using the sparsity constraint depicted in Ref. [11].

3. IMAGE FORMATION MODEL IN 2PE SPECKLE MICROSCOPY

We now turn to the simulation of a 2PE speckle microscopy experiment and the analysis of its resolution in both the transverse and axial planes. We consider a three-dimensional (3D) microscope in which a 3D image of the sample is recorded, by remote focusing [14,15] or using a multifocus scheme [16], for

each illumination. In this case, the image formation model Eq. (1) is applicable in the three dimensions. For each experiment, we simulate 100 images with 100 different speckle realizations using Eq. (1) and deteriorate the result with Poisson noise. The maximum number of photons per Nyquist pixel per speckle image is taken equal to 200.

We call k_0 the wavenumber of the emitted fluorescence that is collected with an objective of numerical aperture NA_{coll} . We assume that the 2PE excitation speckle $I_{2\text{pe}}$ stems from a pulsed laser with a centered wavenumber of $k_0/2$ via an objective of numerical aperture NA_{ill} . Hereafter, we overlook the spectral width of the pulsed laser and use a simple monochromatic description of the speckle patterns. For a 300 fs pulsed laser of wavelength close to 1 μm , this approximation should be valid over several micrometers about the temporal focusing plane [17]. We model the collection point-spread function as $h_{\text{coll}} = h[\text{NA}_{\text{coll}}, k_0]$ and the 2PE speckle as $I_{2\text{pe}} = I^2[\text{NA}_{\text{ill}}, k_0/2]$, where

$$h[\text{NA}, k_0](\mathbf{r}) = C \left| \int_D e^{i\sqrt{k_0^2 - k_{\parallel}^2} z} e^{i\mathbf{k}_{\parallel} \cdot \mathbf{r}_{\parallel}} d\mathbf{k}_{\parallel} \right|^2. \quad (3)$$

$C = 1 / \int h(\mathbf{r}) d\mathbf{r}$, $\mathbf{r} = \mathbf{r}_{\parallel} + z\hat{\mathbf{z}}$ is the space variable with $\mathbf{r}_{\parallel} = x\hat{\mathbf{x}} + y\hat{\mathbf{y}}$ and $\hat{\mathbf{z}}$ is the optical axis. D is a disk of radius $k_0 \text{NA}$ and $I[\text{NA}, k_0]$ is the 1PE speckle pattern,

$$I[\text{NA}, k_0](\mathbf{r}) = \left| \int_D e^{i\phi(\mathbf{k}_{\parallel})} e^{i\sqrt{k_0^2 - k_{\parallel}^2} z} e^{i\mathbf{k}_{\parallel} \cdot \mathbf{r}_{\parallel}} d\mathbf{k}_{\parallel} \right|^2, \quad (4)$$

with $\phi(\mathbf{k}_{\parallel})$ an uncorrelated random variable distributed uniformly between 0 and 2π . $\mathbf{k}_{\parallel} = k_x\hat{\mathbf{x}} + k_y\hat{\mathbf{y}}$ is the transverse wave vector.

For comparison, the 2PE speckle, $I_{2\text{pe}} = I^2[\text{NA}_{\text{ill}}, k_0/2]$, is compared to the 1PE speckle, $I_{1\text{pe}} = I[\text{NA}_{\text{ill}}, k_0]$, in Fig. 1. We observe that the 2PE speckle spots seem about twice larger than of the 1PE ones. Indeed, even though their Fourier supports have roughly the same extension (the doubling of wavelength being compensated for by the squaring of intensity), the 2PE speckle spectrum decays much more rapidly than the 1PE

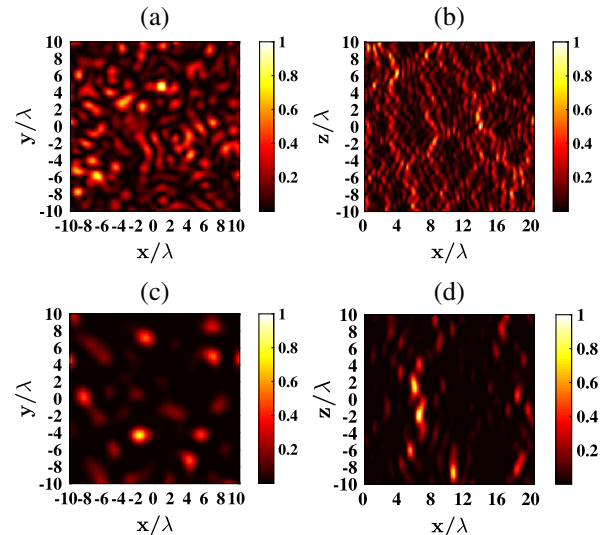


Fig. 1. Speckles obtained with $\text{NA}_{\text{ill}} = 1$. (a) Speckle 1PE (x, y). (b) Speckle 1PE (x, z). (c) Speckle 2PE (x, y). (d) Speckle 2PE (x, z).

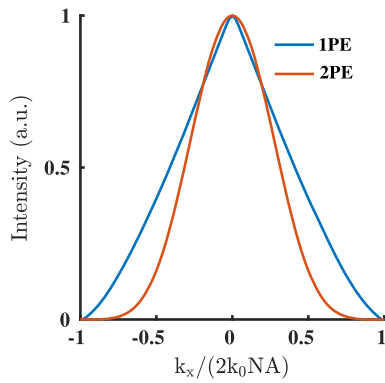


Fig. 2. 1PE and 2PE speckle spectrum (one-dimensional cut).

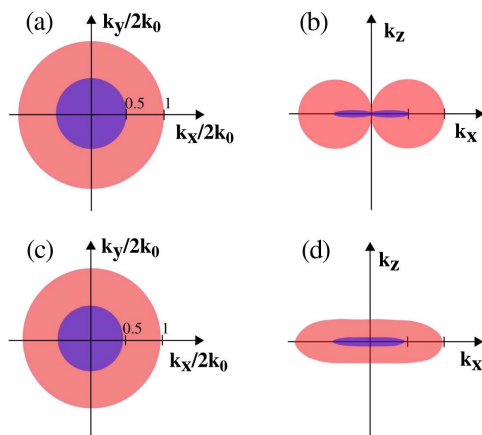


Fig. 3. (a), (b) Fourier supports in the (x, y) and (x, z) planes of the collection point-spread function for $NA = 1$ (pink) and $NA = 0.5$ (blue). (c), (d) Same for the 2PE speckles.

spectrum with increasing frequency, as shown in Fig. 2. On the other hand, the 2PE speckle patterns are significantly sparser than the 1PE ones.

In Fig. 3, we present the Fourier support of the 2PE speckle (bottom row) and that of the collection point-spread function h_{coll} (top row). We observe that the two supports are similar in the transverse plane (left column), whereas in the axial plane, the 2PE speckle spectrum extends beyond that of the collection point-spread function as it covers its missing cone.

These observations indicate the stakes of 2PE speckle microscopy: the fast decay of the 2PE speckle spectrum and its extension beyond the collection point-spread function may be detrimental to the resolution, whereas its pronounced sparsity is an asset for the deconvolution scheme.

4. ANALYSIS OF THE RESOLUTION OF 2PE SPECKLE MICROSCOPY

In what follows, we consider a thin fluorescent layer placed in either the (x, y) or (x, z) plane with the fluorescence distribution $\rho = A(1 + \cos 4\theta)$ (where θ is the polar angle) depicted in Fig. 4. To investigate the resolution gain of 2PE speckle

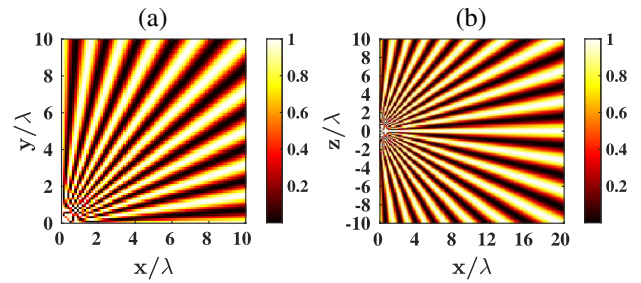


Fig. 4. Sample chosen for the analysis of resolution. It is a thin planar layer with a star-like fluorescence distribution. (a) Study of transverse resolution: the thin layer is placed at $z = 0$. (b) Axial resolution: the thin layer is placed at $y = 0$.

microscopy, we also simulate the images stemming from a bright-field 1PE microscope, $M_{1PE} = \rho * h[NA_{coll}, k_0]$, and the images produced by a classical scanning 2PE microscope, in which the illumination is a focused beam and all emitted photons are collected on a detector, $M_{2PE} = \rho * h^2[NA_{ill}, k_0/2]$. For a fair comparison, these reference images are performed with the same collection and illumination numerical apertures, and the same global photon budget as the speckle experiments. In addition, they are de-convolved using the same algorithm as the one applied to the speckle images.

A. Transverse Resolution

In the transverse (x, y) plane, when $NA_{coll} = NA_{ill} = NA$, the support of the 2PE speckle coincides with that of the collection OTF, which corresponds to the ideal case of the mathematical analysis with ideally a two-fold improvement of resolution. Indeed, we observe that the resolution of the 2PE speckle reconstruction is about 1.5 times better than those of the 1PE wide-field and 2PE scanning images (see Fig. 5). It is roughly

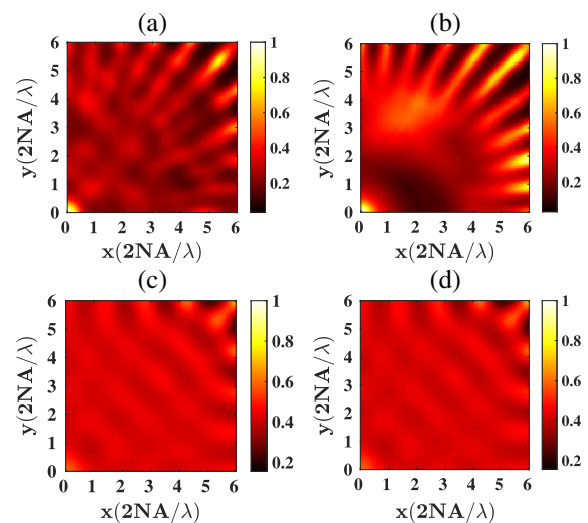


Fig. 5. Transverse resolution with (a) reconstruction obtained in 1PE speckle microscopy, $NA_{ill} = NA_{coll} = NA$. (b) Reconstruction obtained in 2PE speckle microscopy, $NA_{ill} = NA_{coll} = NA$. (c) Reconstruction obtained in 2PE scanning microscopy for a given $NA_{ill} = NA$. (d) Bright-field 1PE.

similar to that obtained in 1PE speckle microscopy as was expected from the similarity of the Fourier supports of excitation and collection. The *a priori* negative impact on the resolution of the more rapid decay of the 2PE speckle spectrum compared with that of the 1PE speckle is not visible on these reconstructions.

We now consider the configuration $NA_{\text{coll}} = NA_{\text{ill}}/2 = NA$ (see Fig. 6). In this case, the transverse support of the speckle exceeds that of the collection OTF. From the mathematical analysis, the identification of the sample spectrum beyond the support of the OTF is not guaranteed anymore. Indeed, comparing Figs. 6(a) and 5(a), we observe that increasing the illumination NA beyond the collection NA does not improve the resolution in the 1PE configuration. On the other hand, in the 2PE case, the resolution of the 2PE speckle image when $NA_{\text{ill}} = 2NA_{\text{coll}}$ is about 1.3 times better than when $NA_{\text{ill}} = NA_{\text{coll}}$, and achieves a two-fold improvement compared with the scanning image [see Figs. 6(b), 5(b), and 5(c)]. The difference in behavior between 1PE and 2PE speckle microscopy when $NA_{\text{ill}} = 2NA_{\text{coll}}$ is striking. The same sample spatial frequencies beyond the observation cut-off are involved in the formation of the 1PE and 2PE speckle images, but the deconvolution algorithm is more efficient on the 2PE speckle images than on the 1PE ones. The former being sparser than the latter (see Fig. 1), it is likely that this achievement comes from a more frequent activation of the positivity constraint on the 2PE images.

This result is promising as it paves the way toward a simple microscopy technique for imaging beyond the diffraction limit. Indeed, one can consider a system where near-field high-frequency speckles are generated (through a silicon wafer [18] or a rough substrate, for example) and the 2PE fluorescence is collected with a standard microscope objective. In this case, resolution improvement better than the standard two-fold gain is feasible.

B. Axial Resolution

We now turn to the analysis of the resolution of speckle microscopy in the axial (x, z) plane. Contrary to the transverse case, the (x, z) support of $\hat{g}_{2\text{pe}}$ extends outside that of $\hat{h}_{1\text{pe}}$ (see Fig. 3). In particular, $\hat{g}_{2\text{pe}}$ covers the missing cone of $\hat{h}_{1\text{pe}}$. This enlarged domain of the 2PE speckle spectrum could be an advantage for the optical sectioning property of 2PE speckle microscopy; however, the identification of the sample spectrum beyond the support of the OTF is not guaranteed.

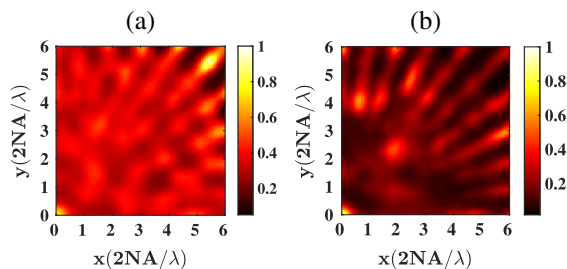


Fig. 6. Study of transverse resolution, $NA_{\text{ill}} = 2NA_{\text{coll}}$. (a) Reconstruction obtained in 1PE speckle microscopy. (b) Reconstruction obtained in 2PE speckle microscopy.

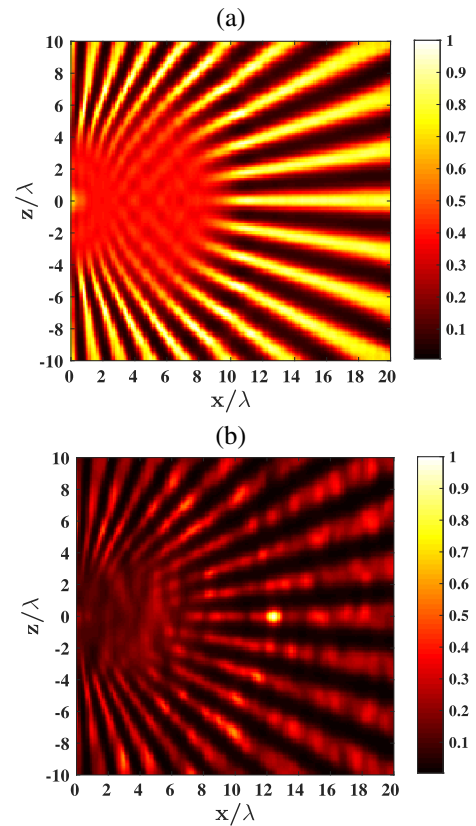


Fig. 7. Study of axial resolution, $NA_{\text{ill}} = NA_{\text{coll}} = 1$. (a) Deconvolution of the image obtained in scanning 2PE microscopy. (b) Reconstruction obtained in 2PE speckle microscopy.

We observe in Fig. 7 that the axial resolution of the 2PE speckle reconstruction is about 1.5 times better than that of the scanning 2PE image. The increase of image sparsity induced by the 2PE speckle illumination, although less visible in the z direction than in the transverse plane, has permitted retrieving some of the sample high spatial frequencies along z axis. Unfortunately, contrary to the transverse case, increasing NA_{ill} beyond NA_{coll} had no impact on the image sparsity along z and did not permit ameliorating the axial resolution (not shown). The bright spot visible in Fig. 7(b) is directly linked to a speckle hot spot at this specific location, which is enhanced by the deconvolution and which would not disappear when taking the mean of the speckle images. Indeed, homogenizing the illumination in average is more difficult in the 2PE configuration than in 1PE because the 2PE speckles are sparser.

5. CONCLUSION

We have presented a numerical analysis of 2PE speckle microscopy, in which a super-resolved image is simply the mean of deconvolved speckle images under a positivity constraint. With such an algorithm, the resolution depends strongly on the sparsity of each speckle image, which is significantly reinforced when using 2PE speckle excitation. With standard optical objectives, the transverse and axial resolutions of 2PE speckle microscopy should be significantly better than those of 2PE

scanning microscopy or 1PE bright-field microscopy. In addition, this technique could be extended to imaging beyond the diffraction limit by using evanescent 2PE speckle patterns formed through a high-index substrate.

APPENDIX A: RECONSTRUCTION PROCEDURE

In this appendix, we briefly sketch the main steps of the deconvolution procedure under a positivity constraint that we applied on the raw speckle images prior to averaging. Following Eq. (1), the fluorescence image of the sample illuminated with a speckle pattern, I_l ($l = 1, \dots, L$), can be modeled as

$$M_l = \mathbf{A}(\rho I_l) + \epsilon, \quad (\text{A1})$$

where ϵ represents the noise and the linear operator \mathbf{A} describes the convolution ($\mathbf{A}(\rho I_l) = \rho I_l * h$). Each image M_l is deconvolved so as to reconstruct the product ρI_l . Introducing the auxiliary variable $q_l = \rho I_l$ for $l = 1, \dots, L$, the deconvolution algorithm can be stated as finding a positive q_l (writing $q_l = \eta_l^2$) so as to minimize the cost functional (no regularization term):

$$\mathcal{F}(\eta_l) = \frac{1}{2} \|M_l - \mathbf{A}(\eta_l^2)\|^2. \quad (\text{A2})$$

Once the q_l are known, the indetermination on ρ and I_l is removed by using the homogeneity constraint on the illuminations $\sum_{l=1}^L I_l = I_0$ to form $\rho = (\sum_{l=1}^L q_l)/I_0$. Minimization of \mathcal{F} is performed using a conjugate gradient method. For each speckle realization, a sequence (η_n) is built up according to the following recursive relation:

$$\eta_n = \eta_{n-1} + \alpha_n d_n, \quad (\text{A3})$$

with η_n and η_{n-1} estimations of η for the iteration steps n and $n-1$, respectively. The function d_n represents the Polak–Ribière conjugate gradient direction,

$$d_n = g_{\eta;n} + \gamma_n d_{n-1}, \quad (\text{A4})$$

with

$$\gamma_n = \frac{\langle g_{\eta;n} | g_{\eta;n} - g_{\eta;n-1} \rangle}{\|g_{\eta;n-1}\|^2}. \quad (\text{A5})$$

The function $g_{\eta;n}$ is the gradient of the cost functional $\mathcal{F}(\eta)$ with respect to η evaluated for the estimation η_{n-1} . This gradient reads as

$$g_{\eta;n} = -2\eta_{n-1} \mathbf{A}^\dagger(v_{n-1}), \quad (\text{A6})$$

where $v_{n-1} = M_l - \mathbf{A}(\eta_{n-1}^2)$ is the residual error at iteration $(n-1)$ and \mathbf{A}^\dagger is the adjoint operator of \mathbf{A} ,

$$\mathbf{A}^\dagger(u) = u * h^t, \quad (\text{A7})$$

where h^t is the transpose of h . Once the updating direction is computed, the real scalar α_n is determined at each iteration step by minimizing the cost function,

$$\begin{aligned} \mathcal{F}(\alpha_n) &= \frac{1}{2} \|M_l - \mathbf{A}(\eta_n^2)\|^2 \\ &= \frac{1}{2} \|v_{n-1} - 2\alpha_n \mathbf{A}(\eta_n d_n) - \alpha_n^2 \mathbf{A}(d_n^2)\|^2. \end{aligned} \quad (\text{A8})$$

Minimization of this cost function, which is a polynomial in α of the fourth order, is achieved analytically.

For all the reconstructions, the initial guess was a constant and the iterations were stopped when the reconstructions began to exhibit noise-induced features (it corresponds to an “eye” regularization [19]). One hundred iterations were generally sufficient for all the presented reconstructions.

Funding. Erasmus Mundus Doctorate Program Europhotonics (159224-1-2009-1-FR-ERA MUNDUS-EMJD); Institut Thématique Multi-Organisme Cancer (ITMO Cancer) (Plan Cancer 2014–2019).

Acknowledgment. Awoke Negash is supported by the Erasmus Mundus Doctorate Program Europhotonics and Anne Sentenac is supported by the ITMO Cancer.

REFERENCES

1. P. T. So, C. Y. Dong, B. R. Masters, and K. M. Berland, “Two-photon excitation fluorescence microscopy,” *Ann. Rev. Biomed. Eng.* **2**, 399–429 (2000).
2. O. Therrien, B. Aubé, S. Pagès, P. De Koninck, and D. Côté, “Wide-field multiphoton imaging of cellular dynamics in thick tissue by temporal focusing and patterned illumination,” *Biomed. Opt. Express* **2**, 696–704 (2011).
3. D. Oron, E. Tal, and Y. Silberberg, “Scanningless depth-resolved microscopy,” *Opt. Express* **13**, 1468–1476 (2005).
4. A. Vaziri and C. V. Shank, “Ultrafast widefield optical sectioning microscopy by multifocal temporal focusing,” *Opt. Express* **18**, 19645–19655 (2010).
5. L.-C. Cheng, C.-Y. Chang, C.-Y. Lin, K.-C. Cho, W.-C. Yen, N.-S. Chang, C. Xu, C. Y. Dong, and S.-J. Chen, “Spatiotemporal focusing-based widefield multiphoton microscopy for fast optical sectioning,” *Opt. Express* **20**, 8939–8948 (2012).
6. M. Ingaramo, A. G. York, P. Wawrzusins, O. Milberg, A. Hong, R. Weigert, H. Shroff, and G. H. Patterson, “Two-photon excitation improves multifocal structured illumination microscopy in thick scattering tissue,” *Proc. Natl. Acad. Sci. USA* **111**, 5254–5259 (2014).
7. P. W. Winter, A. G. York, D. D. Nogare, M. Ingaramo, R. Christensen, A. Chitnis, G. H. Patterson, and H. Shroff, “Two-photon instant structured illumination microscopy improves the depth penetration of super-resolution imaging in thick scattering samples,” *Optica* **1**, 181–191 (2014).
8. B. E. Urban, J. Yi, S. Chen, B. Dong, Y. Zhu, S. H. DeVries, V. Backman, and H. F. Zhang, “Super-resolution two-photon microscopy via scanning patterned illumination,” *Phys. Rev. E* **91**, 042703 (2015).
9. E. Mudry, K. Belkebir, J. Girard, J. Savatier, E. L. Moal, C. Nicoletti, M. Allain, and A. Sentenac, “Structured illumination microscopy using unknown speckle patterns,” *Nat. Photonics* **6**, 312–315 (2012).
10. J. Idier, S. Labouesse, M. Allain, P. Liu, S. Bourguignon, and A. Sentenac, “On the super-resolution capacity of imagers using unknown speckle illuminations,” *IEEE Trans. Comput. Imaging* **4**, 87–98 (2017).
11. S. Labouesse, A. Negash, J. Idier, S. Bourguignon, T. Mangeat, P. Liu, A. Sentenac, and M. Allain, “Joint reconstruction strategy for structured illumination microscopy with unknown illuminations,” *IEEE Trans. Image Process.* **26**, 2480–2493 (2017).
12. J. Min, J. Jang, D. Keum, S.-W. Ryu, C. Choi, K.-H. Jeong, and J. C. Ye, “Fluorescent microscopy beyond diffraction limits using speckle illumination and joint support recovery,” *Sci. Rep.* **3**, 2075 (2013).
13. A. Negash, S. Labouesse, N. Sandeau, M. Allain, H. Giovannini, J. Idier, R. Heintzmann, P. C. Chaumet, K. Belkebir, and A. Sentenac, “Improving the axial and lateral resolution of three-dimensional fluorescence microscopy using random speckle illuminations,” *J. Opt. Soc. Am. A* **33**, 1089–1094 (2016).
14. S. Quirin, D. S. Peterka, and R. Yuste, “Instantaneous three-dimensional sensing using spatial light modulator illumination with extended depth of field imaging,” *Opt. Express* **21**, 16007–16021 (2013).

15. E. J. Botcherby, R. Juškaitis, M. J. Booth, and T. Wilson, "An optical technique for remote focusing in microscopy," *Opt. Commun.* **281**, 880–887 (2008).
16. S. Abrahamsson, J. Chen, B. Hajj, S. Stallinga, A. Y. Katsov, J. Wisniewski, G. Mizuguchi, P. Soule, F. Mueller, C. D. Darzacq, X. Darzacq, C. Wu, C. I. Bargmann, D. A. Agard, M. Dahan, and M. G. L. Gustafsson, "Fast multicolor 3D imaging using aberration-corrected multifocus microscopy," *Nat. Methods* **10**, 60–63 (2013).
17. E. Tal, D. Oron, and Y. Silberberg, "Improved depth resolution in video-rate line-scanning multiphoton microscopy using temporal focusing," *Opt. Lett.* **30**, 1686–1688 (2005).
18. D. Fletcher, K. Crozier, C. Quate, G. Kino, K. Goodson, D. Simanovskii, and D. Palanker, "Near-field infrared imaging with a microfabricated solid immersion lens," *Appl. Phys. Lett.* **77**, 2109–2111 (2000).
19. M. Bertero and P. Boccacci, *Introduction to Inverse Problems in Imaging* (CRC Press, 1998).